# CHAPTER-2

## SYNTHESIS, CHARACTERIZATIONS, AND ANALYSIS TECHNIQUES

# CHAPTER 2: Synthesis, Characterizations, and Analysis Techniques

## 2.1 Overview

To accomplish the objectives discussed in chapter 1, it is essential to synthesize the investigated system and characterize them for their further analysis. This chapter describes the synthesis methods, characterization with distinct techniques, and the applied experimental techniques to evaluate the various properties of the proposed systems. In the present work, the proposed compositions (a) Lanthanum ferrite ($LaFeO_3$),(b) Strontium Titanate ($SrTiO_{3-\delta}$), (c) Srontium doped Lanthanum Ferrite $La_{0.5}Sr_{0.5}FeO_{3-\delta}$ (d) Srontium at A- and Titanium at B-site doped $La_{0.5}Sr_{0.5}Fe_{0.5}Ti_{0.5}O_{3-\delta}$ (d) Heterostructure formed $La_{0.5}Sr_{0.5}Fe_{0.5}Ti_{0.5}O_3/ZnO/La_{0.5}Sr_{0.5}Fe_{0.5}Ti_{0.5}O_3$ were prepared. These compositions were synthesized using a solid-state reaction route (SSR). To conduct a comparative study with the SSR method, the composition $La_{0.5}Sr_{0.5}FeO_{3-\delta}$ was also synthesized via the hydrothermal method. The heterostructure was prepared using the pulse laser deposition technique. Various physical properties including structural, optical, thermal, and electrical characteristics were analyzed for all synthesized materials, along with their electrochemical properties. This chapter has been divided into three sections:

**(1) Materials synthesis:** The sample preparation and processing of materials with various compositions have been discussed in this section.

**(2) Characterization techniques:** This section briefly discusses the structural, microstructural, thermal, optical, and electrical characterization techniques used in the current investigation.

**(3) Data analysis techniques:** In this section, we have outlined analysis techniques, including Rietveld refinement of the X-ray diffraction (XRD) pattern, electrical conductivity, and impedance spectroscopy.

### 2.1.1 Specification of Raw Materials used

High purity raw materials were used to synthesize the investigated compositions. The specifications of raw materials are listed in Table 2.1.

**Table 2.1** Description of the raw materials with their chemical formula, purity, and manufacturer used for the preparation of proposed compositions.

| S. No. | Raw Materials | Chemical Formula | Purity | Manufacturer |
|---|---|---|---|---|
| **1.** | Lanthanum oxide | $La_2O_3$ | 99.9% | Alfa Aesar |
| **2.** | Iron Oxide | $Fe_2O_3$ | 99.9% | Alfa Aesar |
| **3.** | Strontium carbonate | $SrCO_3$ | 99.9% | Alfa Aesar |
| **4.** | Titanium Oxide | $TiO_2$ | 99.9% | Alfa Aesar |
| **5.** | Lanthanum Nitrate | $La(NO_3)_3.6H_2O$ | 99% | Otto |
| **6.** | Strontium Nitrate | $Sr(NO_3)_2$ | 99.9% | Alfa Aesar |
| **7.** | Iron Nitrate Nonahydrate | $Fe_2(NO_3)_3.9H_2O$ | 99.9% | Alfa Aesar |

A few other high-grade chemicals, reagents, and solvents were also used to fabricate the samples like ethanol, acetone, ethylene glycol, nitric acid, deionized water, potassium hydroxide, sodium sulphate, sulphuric acid, hydrochloric acid, etc.

## 2.2 Materials Synthesis

In the present work, in order to synthesize the materials , different synthesis techniques were used. For the heterostructure formation, Pulse Laser Deposition (PLD) was used.

The details of preparative methods, experimental techniques and the basic working principle of the instruments used are discussed in this chapter.

### 2.2.1 Solid-State Reaction Route (SSR)

The solid-state reaction route (SSR) is an extensively used technique for the synthesis of polycrystalline solids and ceramics. It involves mechanical mixing of oxide powders, carbonates, followed by heat treatment. Generally, solids do not react at room temperature and it is necessary to heat them at much higher temperature for the reaction to occur. In this, precursors are weighed and thouroughly mixed in mortar and pestle with acetone and a repetitive process of mixing and grinding takes place till the desired result not obtained. Several factors affect the rate of reaction in this method like reaction conditions, structural properties of the recatants, shape, surface area of the recatants and thermodynamic properties associated with the reaction process[117].There are some advantages associated with this method are listed below:

1. Limited formation of byproducts
2. Structure purity along with desired properties.
3. Large scale production
4. Environment-friendly
5. Simple and low cost

A detailed procedure of the solid-state reaction route is shown in the schematic block diagram of Fig. 2.1.

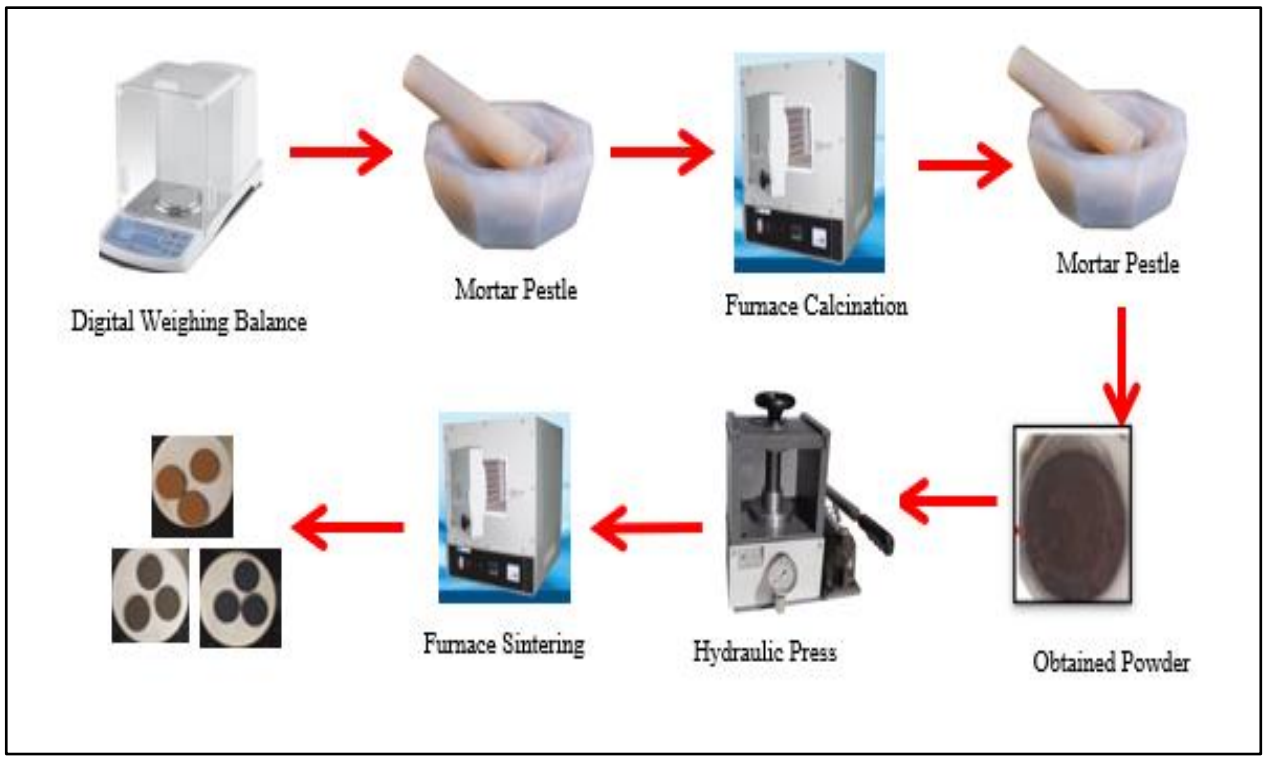


**Figure 2.1** Schematic of Solid-state reaction route.

### 2.2.2 Hydrothermal synthesis route

In 1792, Sir Roderick Murchison employed this technique for the first time to explain the action of water at high temperature and pressure. In this method the heterogeneous reaction occurs in solvents at high temperature and pressure near the critical point in the closed vessel called 'autoclave' yielding the nanostructured particle. The main principle of this technique involves the insoluble material at ambient temperature made soluble under high pressure and temperature[118].

The solution in the Teflon lined steel autoclave is heated over the boiling point of the precursor and desired shape and size of nano particle obtained on the basis of the selected solvent and chemical composition of precursors at required temperature and pressure[119].

This synthesis has various Advantages which are listed below:

- Crystal growth of those materials which have low melting point.
- Crystal growth of those materials which have high vapour pressure near their melting points.
- New phase can access.
- The hydrated and hydroxylated materials can be synthesized.
- Size control of the material with applying desired pressure and temperature.
- This prevent the material/sample with the direct contamination that is why the chance of impurity is less.

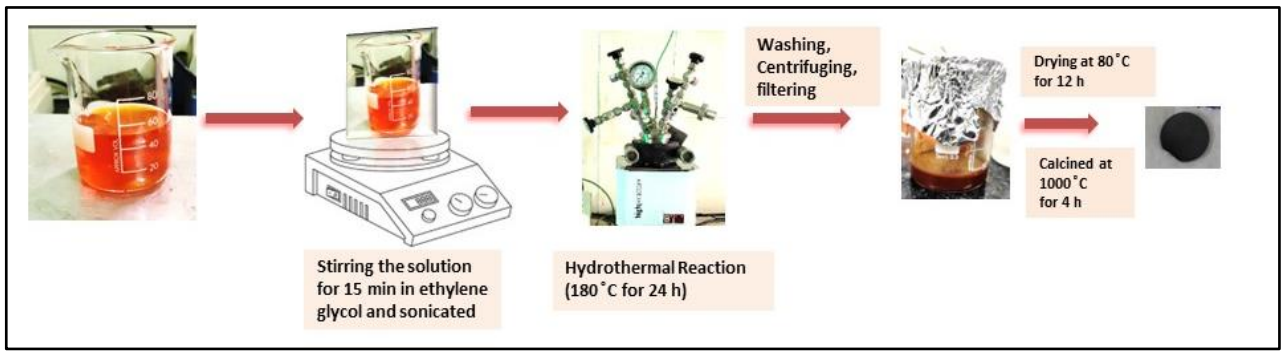


**Figure 2.2** Schematics of Hydrothermal synthesis process.

### 2.2.3 Pulse Laser Deposition Technique (PLD)

Pulse laser deposition (PLD) is a laser ablation technique which is a green method used for the synthesis. Here, a high-power pulsed laser beam is focused to strike a target of the desired composition. Material is then vaporized and deposited as a thin film on a substrate facing the target[120]. All this process occur in the ultra-high vacuum (UHV) or in the presence of desired gas. PLD equipment COMPex 102 F is used in this study. The experimental setup and the specification are mentioned in Fig 2.3. The laser used was a Kr:F excimer laser,

operating at a wavelength of 248 nm. The stainless-steel chamber mainly comprises of the target holder, heating equipment and the substrate holder.

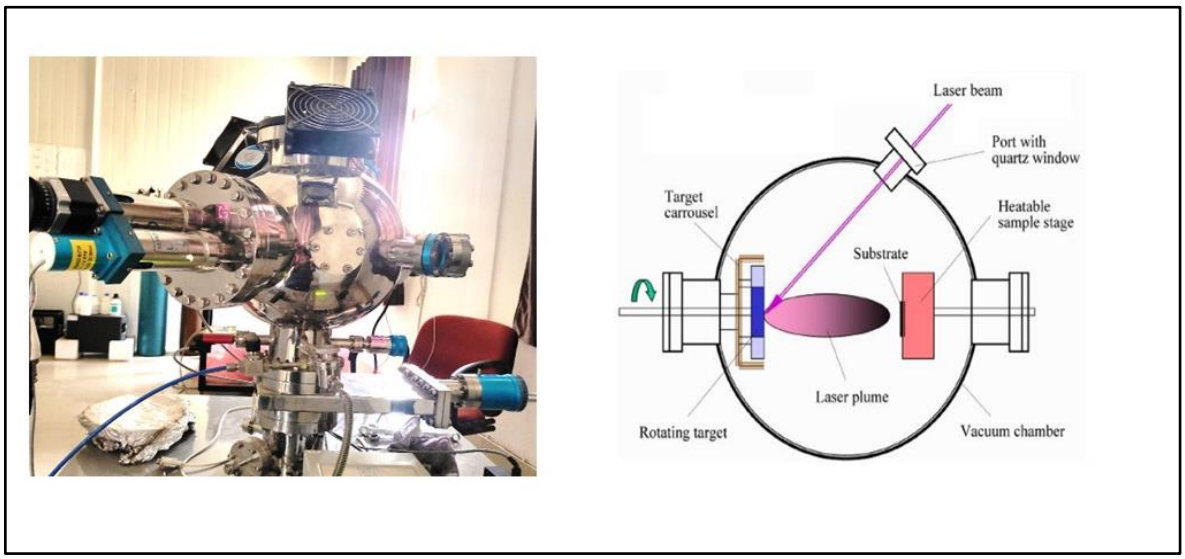


**Figure 2.3** PLD experimental set-up and schematics of Pulse laser deposition process.

The laser beam was incident on the rotating target at a 45° angle, after passing through the focusing lens controlled by a stepper motor. The vacuum chamber was evacuated using both mechanical rotary pump and a turbo-molecular pump[121].

The deposition of thin films can be divided into four stages-

1. Laser-target interaction
2. Plasma plume formation
3. Accumulation of ablated material onto the substrate
4. Nucleation and growth of thin film on the substrate surface

## 2.3 Characterization Techniques

This thesis aims at the study for efficient electrode materials and their catalyst study for oxygen evolution reaction (OER), oxygen reduction reaction (ORR) and hydrogen evolution reaction (HER). The present chapter deals with the characterization techniques adopted to understand the properties and evaluate the performance as the electrode materials as well as the bifunctional catalyst. The upcoming section will delve into the overview and specific of techniques.

### 2.3.1 Thermal Analysis (TGA-DSC)

TGA stands for Thermogravimetric Analysis is an analytical technique used for the determining the thermal stability of the materials. It is also used for the study of thermal decomposition, degradation and the stability properties of materials. It is used to determine the change in mass of the sample as a function of temperature or time under controlled atmosphere (Using gases $N_2$ or He or air or $O_2$). TGA experiment is performed by heating the sample in a certain atmoshphere like nitrogen or oxygen and recorded the weight loss occurred in the sample as the function of temperature. The weight loss is the fundamental properties of the sample which can be used for quantitative calculations of compositional changes[122]. This technique can also verify the phase transition occurred in the sample. TGA experiment in this thesis were performed using TGA/DSC 1 (Mettler Toledo, Germany) model in the nitrogen and oxygen atmosphere and operated within the temperature range from 27 ºC-1000 ºC. The experimental setup of the TGA/DSC technique are shown in Fig. 2.4.

Differential Scanning calorimetry (DSC) method is a thermo-analytical approach that measures the heat flow between a sample and its surrounding as a function of temperature or

time in a controlled temperature regime. The specimen and the reference material are placed symmetrically within the furnace. The known mass of the specimen undergoes heating or cooling, and during this procedure, the variation in heat capacity is recorded in form of heat flow. It is used to determine various material properties such as glass transition temperature, crystallization, thermal stability, specific heat capacity, purity, and oxidation behavior[123].

**Figure 2.4** The experimental setup of TGA/DSC.

### 2.3.2 X-Ray Diffraction Analysis (XRD)

The powder X-ray diffraction (XRD) is a useful technique which is primarily used for phase identification of a crystalline material. It is a non-destructive and versatile analytical approach used for determining important properties like lattice parameters, geometry, orientation and defects of the crystalline materials. When the X-rays are incident on the sample, the atoms will scatter the waves, causing them to interact constructively and resulting in the formation of a diffracted beam. Different materials produce unique XRD patterns, enabling indexing that aids in identifying the various phases present within the material. Commonly, the X-ray radiations are emitted by copper specimen, and its characteristic wavelength is 1.5418 Å for Kα radiation. In this thesis, XRD pattern was recorded using an X-ray diffractometer

(Rigaku Miniflex II) applying Cu-Kα radiation with Ni filter and applied voltage of 40 kV shown in Fig 2.5 (a).

The XRD method follows Bragg's law of X-ray diffraction. This law can be explained geometrically, as depicted in Fig. 2.5(b). A collimated beam of X-rays is incident on the crystallographic lattice plane with an interplanar spacing $d_{hkl}$ at a certain incidence angle θ (between the incident and the scattered rays) and it create a path difference of $2d_{hkl}Sin\theta$. If this path difference is equal to an integral multiple of wavelength ($\lambda$), then the constructive interference ocuured between these scattered rays. This condition of constructive interference follows the Bragg's law and is given by[124]:

$$2d_{hkl}\text{Sin}\theta = n\lambda \quad (2.1)$$

where n is diffraction order in integer.

In some of the cases, the X-ray source is kept at a stationary position while the sample and detector rotated by angle $\theta$ and $2\theta$, respectively. However, in many cases, the sample retains a stationary position while both the detector and source simultaneously rotate by $\theta$ angle. Normally, the $2\theta$ range between 20° - 80° is sufficient to cover the most useful part of the diffraction pattern.

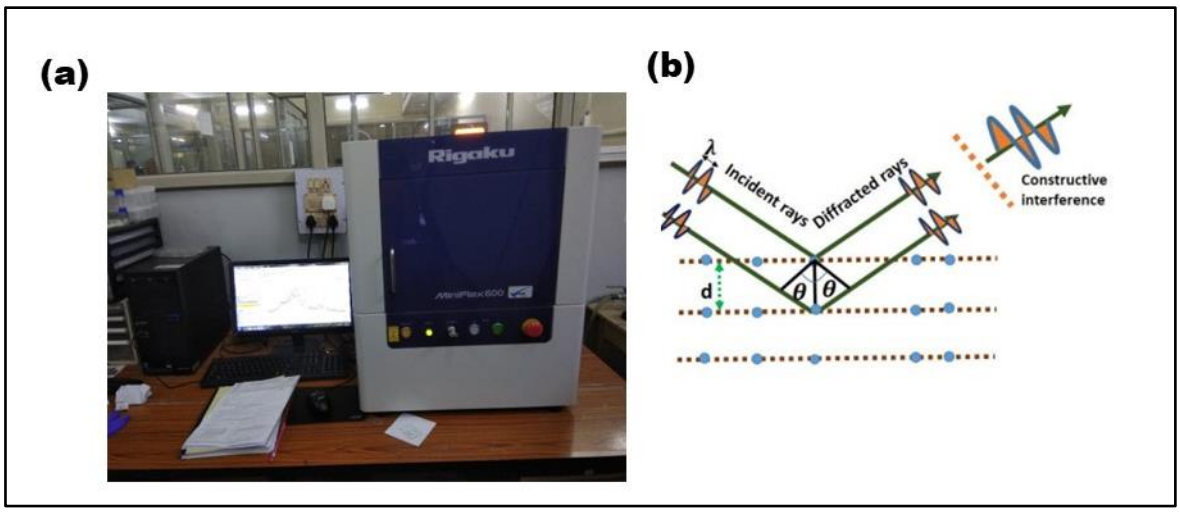


**Figure 2.5 (a)** Experimental setup of X-ray diffractometer [Rigaku Miniflex II, Japan] **(b)** Schematic representation of X-rays diffraction in a crystalline lattice.

For the phase identification, the X-ray diffraction spectra are matched and indexed with the standard reference pattern. This standard database is maintained by "International Center for Diffraction Data (ICDD)" also known as the "Joint Committee for Powder Diffraction Standards (JCPDS)".

In addition, the XRD pattern can also be used to determine the crystallite size $(D)$ of a material using the Scherrer formula equation 2.2 [125]. The Scherrer's formula is given by

$$D = \frac{0.9\,\lambda}{\beta \cos\theta} \tag{2.2}$$

where 0.9 is Scherrer's constant, $\lambda$ wavelength of X-ray source (0.154 nm for Cu-Kα, $\beta$ is FWHM in radians.

For the Rietveld refinement analysis of the XRD pattern FullProf suite software was used, which is thoroughly discussed later in this chapter.

## 2.3.3 Fourier Transform Infrared Spectroscopy (FTIR)

Infrared spectroscopy is an important technique for the study of absorption, emission and infrared inelastic scattering of the material. This method is used to identify the organic or inorganic compounds absorbed or transmitted through the sample[126]. A schematic diagram and the mechanism of the Fourier transform infrared spectroscope used in our work is shown in Fig. 2.6.

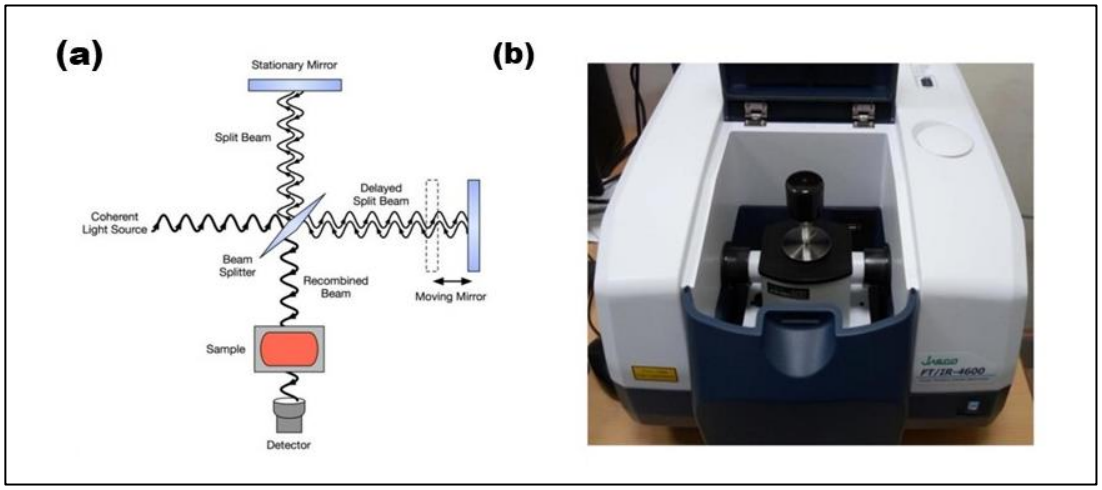


**Figure 2.6 (a)** Mechanism and **(b)** experimental setup of Fourier transform infrared spectroscopy [JASCO 4600].

A Michelson interferometer is usually used in the FTIR spectrometer which consists two mirrors and a beam splitter. One of the mirrors placed and fixed at an angle of 45º, the other one is a movable mirror. The beam is adjusted by changing one of the mirrors with the change in wavelengths that passes through it and produces new data points. Light from the source is combined and routed to the beam splitter in an interferometer which produces a signal in the form of cosine Fourier transform of the spectrum. Within an order of second, the obtained data is Fourier transformed to the recognizable form.

Here in this work the FTIR data was recorded from Jasco FT/IR-4600 spectrometer equipped with an interferometer, high intensity ceramic source, and D1aTGS detector. Analysis of sample was conducted using Attenuated Total Reflectance (ATR). This set-up does not require any pre-prepartion before the experiment and independent of the sample thickness and condition.

### 2.3.4 X-Ray Photoelectron Spectroscopy (XPS)

XPS is a surface-sensitive spectroscopic technique based on the principle of the photoelectric effect. It is used for the elemental composition, identification of chemical and electronic state, of the elements present within the material. It is also used for the identification of the active sites, surface contamination, oxide layers on non-oxide materials, oxidation state etc. A ultra-high vacuum (UHV) chamber typically ~ $10^{-10}$ Torr is used for the investigation of the sample in this technique. This technique is based on the principle of the photoemission in which the material surface is exposed with the high energy X-ray[127]. This results in the ejection of the inner level electrons of the surface atom. These emitted electrons exhibit certain kinetic energy $E_k$ which is used to find the binding energy of those electron (Fig. 2.7). The binding energy can be determined by the following equation:

$$E_B = h\nu + E_k - \Phi \tag{2.3}$$

where, $h\nu$ is the incident energy of X-ray source, $E_k$ is the kinetic energy of emitted electrons, $\Phi$ is the work function of the specific surface of the material, and $E_B$ is the binding energy of core electrons. The removal of the core electron create a hole behind it and an outer electron occupies that core hole. This emits the Auger electron which is again utilized with the emitted

photoelectrons (refer Fig 2.7(a)). Common sources of X-rays are magnesium (Mg-Kα $h\nu = 1.25\ keV$ ) and aluminium (Al-Kα $h\nu = 1.49\ keV$) because of their high energy[128].

XPS is also known as ESCA (Electron Spectroscopy for Chemical Analysis). In Laboratory XPS easily identifies all the elements except hydrogen and helium. Due to unique binding energies associated with each element, XPS measurement can accurately and easily detect the presence of individual elements[129].

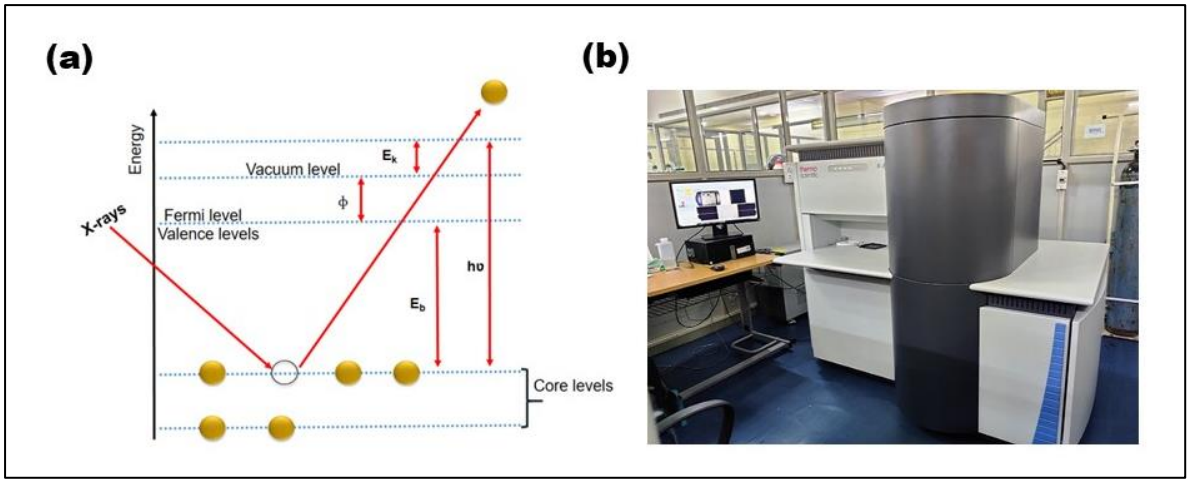


**Figure 2.7 (a)** Mechanism and **(b)** Experimental setup for the XPS spectroscopy (Kratos Amicus).

In this thesis work, XPS spectra of the samples have been recorded using Kratos Amicus XPS setup utilizing Mg target under $10^{-6}$ Pa pressure. The data is calibrated using C1s (284.6 eV) as the reference. The XPS41 software used to deconvolute the spectra with the best fit for the analysis of the sample's properties.

### 2.3.5 Scanning Electron Microscopy (SEM)

SEM is a microscope that uses a focused beam of high-energy electron instead of light to produce images of the sample. It has many advantages over traditional microscopes typically used for research purposes. When a high-energy electron beam is bombarded onto the sample's

surface, it provides high-resolution morphological images and reveals the chemical composition of the material[130][131]. Figure 2.8(a) illustrates electron-sample interactions.

The sample should be conductive for the bombardment of electron beam otherwise a layer of gold is deposited in the case of nonconducting samples[130].

Scanning Electron Microscope consists of different parts, such as an electron source, electromagnetic lenses that focus the generated electron beam on the specimen, an electron detector and image processeor. An electron beam of energy range of 5 to 30 keV, upon striking on the sample, emits different types of electrons and photons from the sample's surface[131]. Due to the inelastic scattering of incoming electrons with the atoms of the sample, secondary electrons are produced, which can be readily detected by the appropriate detector.

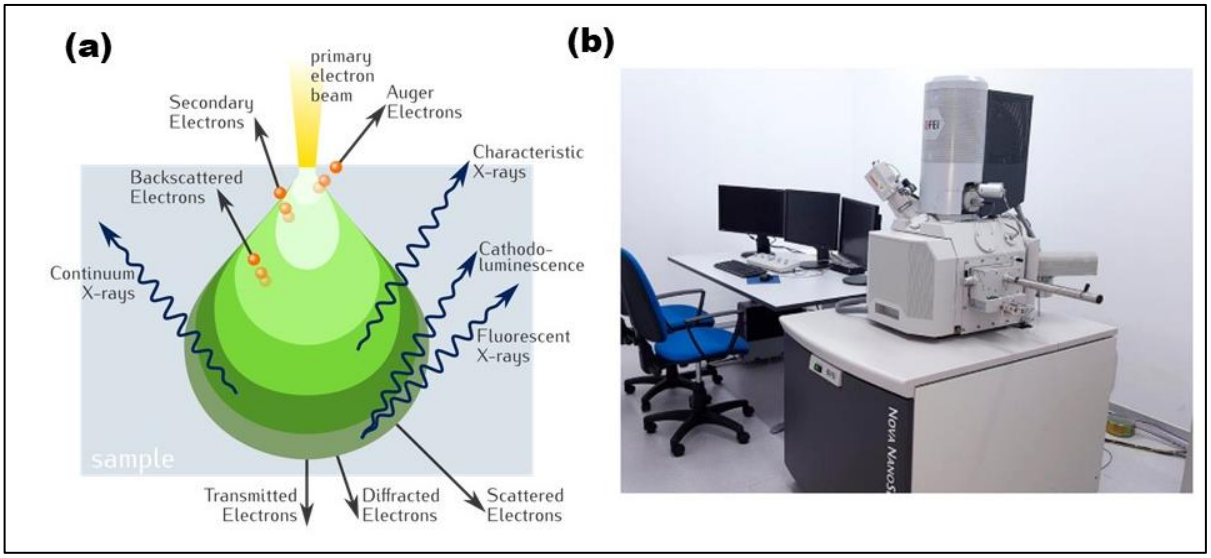


**Figure 2.8 (a)** Mechanism and **(b)** Experimental setup of SEM measurement [Nova Nano SEM 450].

For elemental composition analysis, energy dispersive X-ray analysis (EDAX or EDX) is used. This is based on the principle of Moseley's law and is a non-destructive process. The X-ray generated during the displacement of the electrons from the higher to lower energy shell have

unique energies, which helps in the identification of each element within a sample[132]. It also provides information on the atomic and weight percentages of each element's concentration in the sample[131]. With SEM, this technique does not require any preparation.

In the present thesis, Nova Nano SEM 450 scanning electron microscope has been used for the SEM and for EDS 51N1000-EdS system used for the analysis of the samples, represented in Fig. 2.8(b).

### 2.3.6 Ultra – Violet Visible (UV-Vis) Spectroscopy

UV-Vis is an effective technique for investigating the absorption or reflectance spectra of a sample in the ultraviolet-visible spectral region. It quantifies the attenuation of the light beam after its reflection or transmission from the surface of the sample[133]. Absorbance (A) measures the ratio of incident radiation $(I_o)$ from the source to the refracted radiation detected by detector $(I)$. Transmittance $(T)$ is the ratio of $I$ to $I_o$ which measure the amount of radiation passing through the sample:

$$\mathrm{A} = log_{10}\left(\frac{I_0}{I}\right) = log_{10}\left(\frac{1}{T}\right) \tag{2.4}$$

The measurement of the absorption spectra of the sample is performed using a spectrophotometer[134]. In this thesis, we conducted the experiment using the Jasco V-770 UV-Vis-NIR spectrophotometer (refer to Fig 2.9). It consists of four main components that are radiation source, a sample holder, a diffraction grating in a monochromator, and a detector. The radiation source usually includes a tungsten filament, a deuterium arc lamp, and a Xenon arc lamp. In this case, there are two radiation sources: a deuterium arc lamp as a UV source (190 nm to 400 nm) and a halogen lamp as a visible and NIR source (300 nm to 2500 nm). For a detector a photomultiplier tube is used, to detect the radiations[135]. A UV-Vis

integrating sphere which is coated with barium sulphate from the inside, is used to analyze the absorption spectrum of the sample. The scanning monochromator goes through every wavelength using a "Step-through" process so that intensity can be measured as a function of wavelength[133].


**Figure 2.9** Experimental setup of UV-Visible measurement [JASCO V-770 UV–Vis spectrophotometer].

The absorption spectra are also used to determine the optical band gap ($E_g$) of the material with the help of Tauc relation[136]. For optical band gap estimation, the Tauc relation is given as follows:

$$\alpha h\nu = A\left(h\nu - E_g\right)^n \tag{2.5}$$

where, $h\nu$ is photon's energy, $\alpha$ is absorption coefficient, $A$ is a constant, and $E_g$ represents the optical band gap. Here, $n$ denotes the nature of allowed transition in the material which depend on the type of material. It gives the values: for allowed direct transition $n = 1/2$, $n = 2$ for allowed indirect transitions and $n = 3$ for indirect forbidden transition and $n = 3/2$ for direct forbidden transition[137].

### 2.3.7 Transmission Electron Microscopy (TEM)

The specifications of the microscopes like magnifications and resolutions, vary from one to another. The transmission electron microscope (TEM) is one of the powerful microscopes compared to others used in research. It finds a wide range of applications in research. TEM is a technique where a highly focused electron beam is transmitted through an ultra-thin sample, about 100 nm which interact with the sample as the electron passes through it. It provides both the image and the diffraction of the sample with high lateral spatial resolution. This is used to obtain a complete morphological, crystallographic, chemical composition, bonding, electronic structure and coordination number information from the samples[138][139]. The schematic representation is shown in Fig 2.10(a).

The main components of the TEM consist of sample stage, electron gun, electron lens, apertures, and electrostatic plates. The sample required for analysis is prepared by depositing the dispersed sample onto a copper grid. Grid materials such as copper, molybdenum, or gold can be used[140]. In our thesis, a copper grid is used for analysis because it is non-reactive for the magnetic lens used in the TEM.

TEM microscopy has two different modes: bright field and the dark field, depending on the electrons recorded by the detector. The commonly used bright field imaging exhibit contrast due to the occlusion and absorption of electrons in the sample. TEM images collected from the TECNAI G2 20 TWIN transmission electron microscope used in this work for the study of morphology and particle size of the sample.

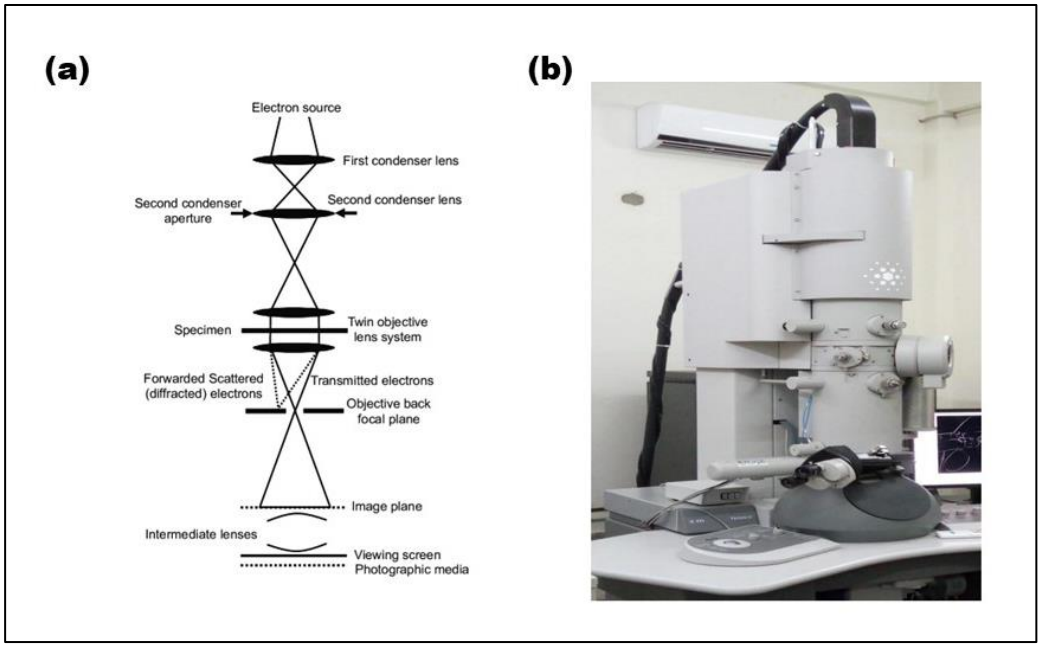


**Figure 2.10 (a)** Mechanism **(b)** Experimental setup of TEM measurement [TECNAI G2 20 TWIN].

SAED stands for Selected Area Electron Diffraction, is also studied alongside TEM. It is used to identify the crystal structure and measure the crystallinity, lattice parameters, and phase identification of samples. Each SAED pattern indicates a diffraction pattern specific to the sample. For example, simple spot patterns correspond to single-crystal diffraction while ring-type patterns correspond to polycrystalline diffraction[141].

The main difference between TEM and SEM, is path of electron. In the case of SEM, unlike TEM, it scans over the surface of the sample to study its morphology[139].

### 2.3.8 Atomic Force Microscopy (AFM)

Atomic Force Microscopy (AFM) was initially showcased by Binning, Quate, and Gerber in 1985 as and advanced non-optical imaging method[142]. AFM enables precise and non-invasive assessment of various characteristics such as topography, electrical conductivity, magnetic behavior, chemical composition, optical properties and mechanical attributes of a

sample surface with exceptional resolution[143]. It is a scanning probe microscopy (SPM) technique renowned for its high resolution, also referred to as scanning force microscopy (SFM).

In a standard AFM system with optical feedback shown in Fig 2.11(a), the fundamental operating principle involves scanning an AFM probe, equipped with a sharp tip,across a sample surface in a raster pattern. Typically composed of silicon or silicon nitride , the AFM tip is integrated near the free end of a flexible AFM cantilever. A piezoelectric ceramic scanner governs both lateral and vertical movements of the AFM probe relative to the surface. As the AFM tip traverses features of varying heights, the deflection of the AFM cantilever and directed onto a position-senistive photodetector. A Feedback loop regulates the vertical displacement of the scanner to maintain a nearly constant deflection of the AFM cantilever, thereby ensuring a consistent interaction force. The coordinates traced by the AFM tip during scanning are compiled to construct a three-dimensional topographic representation of the surface.

AFM find application in various fields such as solid-state physics, polymer physics, medicine, nanotechnology, material science, electronics and optoelectronics due to its applicability to provide high-resolution imaging and precise measuremnets of surface properties. In this work, the sample's morphology was examined using AFM instrument by NTEGRA Prima of NT-MDT service (Fig. 2.11(b)).

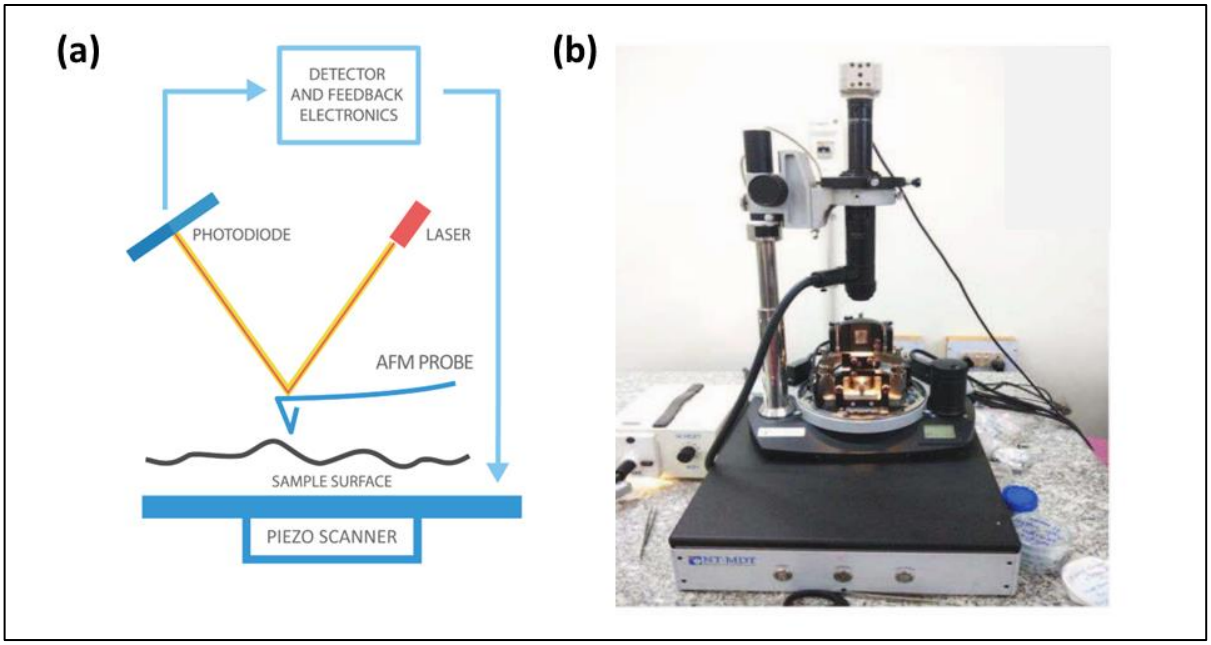


**Figure 2.11 (a)** Schematics of AFM **(b)** Experimental Set-up of AFM.

### 2.3.9 Density Measurement

With the help of Archimedes principle, we estimated the density of the sintered sample in pellet form. Firstly, the pellets are weighed in the air and then weighed in water as a liquid medium. In this thesis, the experiment was performed using the Sartorius, BSA2245-CW density measurement kit, depicted in Fig. 2.12. The equation used in the experiment is given as follows:

$$D = \frac{w_1}{w_2} \times \rho, \tag{2.6}$$

where $D$ is the density of the sample used, $w_1$ is the weight of the sample, $w_2$ weight of the water displaced, $\rho$ is the density of water.

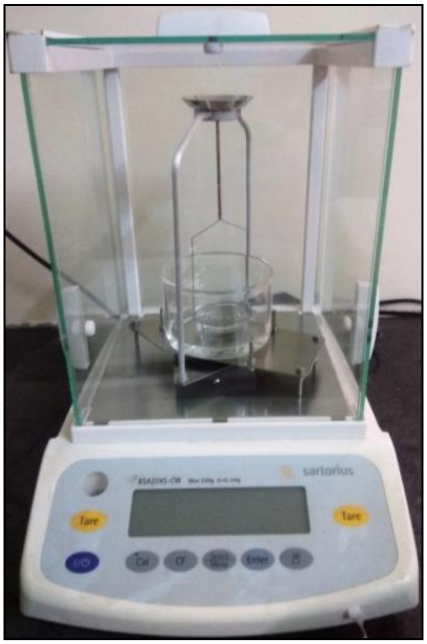


**Figure 2.12** Density measurement kit by Sartorius, BSA2245-CW.

Theoretical density was obtained from the molecular weight of given compound and lattice parameters by using the above relation-

$$D_{th} = \frac{n \times M}{N \times V} \tag{2.7}$$

where $D_{th}$, *is* theoretical density, $n$ number of formulas per unit cell, $M$ molecular weight of the given compound, $N$ Avogadro's Number, $V$ unit cell volume.

## 2.4 Electrical Data Analysis

In this thesis the electrical data analysis of the compositions was studied by two methods:

### 2.4.1 Conductivity Spectra

The electrical conductivity spectroscopy is an important technique for studying the conductivity behavior of the sample. Understanding the dynamics of charge carrier involved

in conducting materials is crucial for optimizing their properties. This can be studied using both conduction and modulus spectra [144]. The conductivity, $\sigma'$ of a conductor can be defined in terms of Jonscher's power law:

$$\sigma' = \sigma_{dc} + A\nu^{\eta} = \sigma_{dc}\left[1 + \left(\frac{\nu}{\nu_h}\right)^{\eta}\right] \quad (2.8)$$

where, $\sigma_{dc}$ is the frequency-independent conductivity, $A$ is constant, $\nu$ is the frequency, $\nu_h$ is the hopping frequency, $\eta$ is the power-law exponent, and represents the degree of interaction between the mobile ions with the lattice[145][146].

The hopping frequency, $\nu_h$ and the dc conductivity are related to each other according to the Nernst-Einstein relation:

$$\sigma_{dc} = en_c\mu = \frac{n_c e^2 \gamma \lambda^2}{kT}\nu_h \quad (2.9)$$

where $n_c$ is the concentration of mobile charge carriers, $e$ is the electronic charge, $\mu$ is mobility, $T$ is temperature, $\lambda$ is hopping distance, $\gamma$ is the geometrical factor for ion hopping, and $k$ is Boltzmann's constant. The above equation facilitates the estimation of charge carrier concentration and its dependence on temperature variations. It has been previously studied that the conductivity spectra of ion-conducting materials adhere to the time-temperature superposition principle (TTSP) across various temperatures. This principle indicates that the conductivity isotherm can be superimposed onto a single curve using suitable scaling parameters. This can be mathematically inferred as[147]:

$$\frac{\sigma'(\nu)}{\sigma_{dc}} = F\left(\frac{\nu}{\nu_h}\right) \quad (2.10)$$

here, $F$ is a temperature-independent function, $\nu_h$ is a temperature-dependent scaling parameter. There are number of scaling proposed by various researchers such as Summerfield scaling[148], Roling et al. scaling [149], Sidebottom scaling[150], and Ghosh scaling[147]. The variations among these lie only in the selection of scaling parameters used for each model, i.e., hopping frequency. For Summerfield scaling $\sigma_{dc}T$ is used, in Roling et al., scaling $\frac{\sigma_{dc}T}{\chi}$ is used and for Ghosh scaling $\nu_h$ is used as the scaling parameter. Out of all the mentioned scaling methods, Ghosh scaling has extensive applicability because of its automatic consideration of changes in permittivity[147].

In the composition used in this work, the conductivity spectra consist of plateaus and dispersion region. These plateaus in the low-frequency region suggest the total or bulk conductivity known as $\sigma_{dc}$ while the successive dispersion region represents the combined effect of grain conductivity and the grain-boundary relaxation behavior. If another plateau appears after this dispersion region, it suggests the grain's contribution to the bulk conductivity. Additionally, another dispersion region after this second plateau in the high-frequency region corresponds to the dielectric contribution in the grain relaxation behavior. Therefore, the conductivity spectra define two parts in which the first relates to the frequency-independent part caused by the random motion of charge carriers called dc conductivity, and the second part relates to the frequency-dependent aspect caused by the hopping motion of charge carriers in grains and grain boundaries.

In this work, 6500 P Wayne kerr and the solatron impedance analyzer is used for the analysis of the conductivity spectra data (refer Fig 2.13).

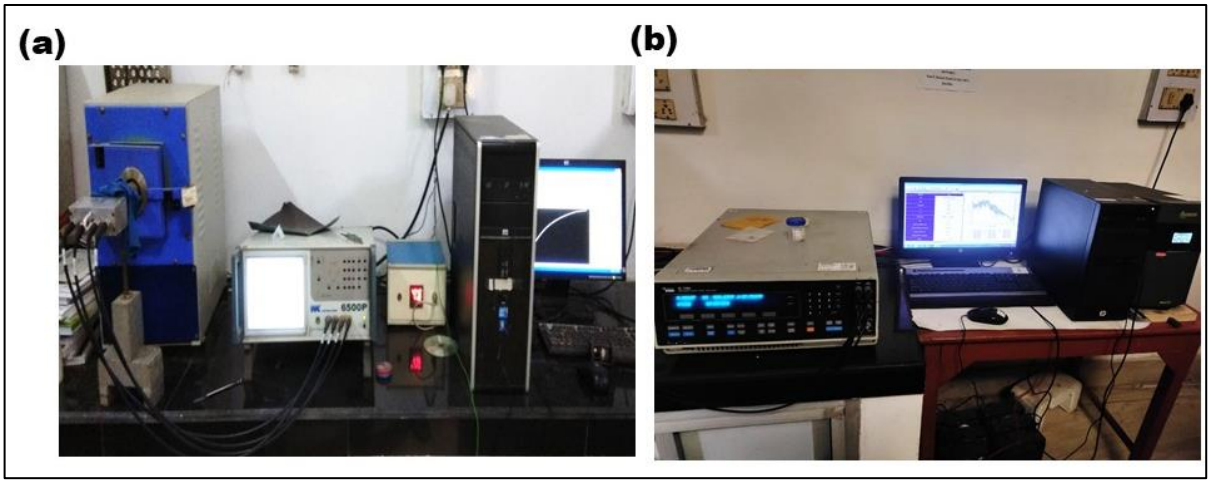


**Figure 2.13** Experimental set up of automated impedance analyzer along with sample holder and furnace **(a)** 6500 P Wayne Kerr, UK **(b)** Solatron, SI 1260 Impedance analyzer, Ametek.

## 2.4.2 Impedance Spectroscopy Analysis

Impedance spectroscopy is a powerful non-destructive technique used to measure the electrical properties of a material. It is valuable for inspecting defects, microstructure, electrical conductivity, and surface chemistry of materials, including dielectrics, ionic conductors, and interfaces between adsorbates and adsorbent[147]. When applying an alternating voltage or current to the sample, information regarding conductivity, impedance, dielectric properties, and modulus properties is obtained [151][147].

For the measurement of the electrical properties of the sample, a pellet of the sample coated with the platinum was cured at 700 ℃ for 30 minutes. Electrical responses such as dielectric constant, impedance, dielectric loss, complex modulus, etc., were measured with the help of Wayne Kerr 6500P series LCR meter and the solatron, SI 1260, impedance analyzer, (Ametek) in the temperature range of RT to 700 ℃ and a frequency range from 0.1 Hz to1 MHz. These studies help in understanding ion relaxation and dynamics phenomenon.

Impedance analysis is a powerful technique to study the different contributions present in the electrical/dielectric properties of ceramics[151]. Compared to direct current, alternating current can resolve all polarization mechanisms by varying the frequency. Impedance is a vector quantity ($Z^*$), and so are electric modulus ($M^*$), admittance ($Y^*$), and permittivity ($\varepsilon^*$). All these consist of real and imaginary component and are related to each other as:

$$Z^* = Z' - iZ'' = \frac{1}{i\omega C_0 \varepsilon^*} \tag{2.11}$$

$$Y^* = Y' + iY'' = i\omega C_0 \varepsilon^* \tag{2.12}$$

$$M^* = M' + iM'' = \frac{1}{\varepsilon^*} \tag{2.13}$$

$$\varepsilon^* = \varepsilon' - i\varepsilon'' \tag{2.14}$$

There are two main plots for impedance analysis, Complex plane plot, like, $Z''$ vs $Z'$ and $M''$ vs $M'$ plots and the Spectroscopic plots like, $\frac{Z''}{Z'}$ or $\frac{M''}{M'}$ vs $log\nu$ plots[152].

For the different analysis, impedance complex quantity $Z^*$ can easily convert to other complex forms summarize in Table 2.2.

**Table 2.2** All detailed relations of complex quantities[153].

| | $\boldsymbol{M^*}$ | $\boldsymbol{Z^*}$ | $\boldsymbol{Y^*}$ | $\boldsymbol{\varepsilon^*}$ | $\boldsymbol{\sigma^*}$ |
|---|---|---|---|---|---|
| $\boldsymbol{M^*}$ | $M^*$ | $i\omega C_o Z^*$ | $i\omega C_o / Y^*$ | $1/ \boldsymbol{\varepsilon^*}$ | $i\omega C_o / \sigma^*$ |
| $\boldsymbol{Z^*}$ | $M^*/i\omega C_o$ | $Z^*$ | $1/ Y^*$ | $1/ i\omega C_o \boldsymbol{\varepsilon^*}$ | $\varepsilon_o / \sigma^* C_o$ |
| $\boldsymbol{Y^*}$ | $i\omega C_o / M^*$ | $1/Z^*$ | $Y^*$ | $i\omega C_o \boldsymbol{\varepsilon^*}$ | $\varepsilon_o \sigma^* / C_o$ |
| $\boldsymbol{\varepsilon^*}$ | $1/ M^*$ | $1/ i\omega C_o Z^*$ | $Y^* / i\omega C_o$ | $\varepsilon^*$ | $\sigma^* / i\omega \varepsilon_o$ |
| $\boldsymbol{\sigma^*}$ | $i\omega \varepsilon_o / M^*$ | $\varepsilon_o / C_o Z^*$ | $Y^* \varepsilon_o / C_o$ | $i\omega \varepsilon_o \varepsilon^*$ | $\sigma^*$ |

A ceramic sample has contributions of grains, grain boundary, and electrode. Each contribution represented by an equivalent circuit containing resistance, *R* and capacitance, *C*. Nyquist plot or previously known as Cole-Cole plot has widespread application in determining the frequency response information of a system through the complex impedance function:

$$Z^*(\omega) = Z'(\omega) - iZ''(\omega) \tag{2.15}$$

where $Z'(\omega)$ and $Z''(\omega)$ are the real and imaginary part of complex quantity $Z^*(\omega)$. These real and imaginary part of total impedance is given by:

$$Z' = \frac{R_b}{1+(\omega R_b C_b)^2} + \frac{R_{gb}}{1+\left(\omega R_{gb} C_{gb}\right)^2} + \frac{R_{el}}{1+(\omega R_{el} C_{el})^2} \tag{2.16}$$

$$\text{Z''} = \frac{\omega C_b R_b^2}{1+(\omega R_b C_b)^2} + \frac{\omega C_{gb} R_{gb}^2}{1+\left(\omega R_{gb} C_{gb}\right)^2} + \frac{\omega C_{el} R_{el}^2}{1+(\omega R_{el} C_{el})^2} \tag{2.17}$$

where, $R_g$ , $R_{gb}$ , $R_{el}$ are the grain resistance, grain boundary resistance and electrode resistance, respectively and $C_g$, $C_{gb}$, $C_{el}$ are the capacitance of grain, grain boundary, and electrode respectively[154].

In impedance and modulus analysis, semicircular arcs may be observed, each representing contributions from relaxation time. Like in Fig 2.14, three semicircular arcs means three contributions involved and having single value of relaxation time. This Relaxation time ($\tau$) is inverse of angular frequency ($\omega$) at which the relaxation peaks occurred and inferred as:

$$\tau = 1/\omega = RC \tag{2.18}$$

The point where the arcs intersect with the real axis ($M^{'}$) provide the $R_g$, $R_{gb}$, and $R_{el}$'s contributions in the impedance plots. These are inversely proportional to the capacitive contributions ( $C_o/C_g, C_o/C_{gb}$ *and* $C_o/C_{el}$) in the modulus plot. Electrode polarization

emerges in the lowest frequency range within the complex impedance plot, followed by grain boundaries in the mid frequency range, and grain contribution emerges in the highest frequency range. If the center of the above three semicircle aligns with the real axis, specifically $Z'$ and $M'$, then it suggests that all contributions possess a uniform relaxation time value. Conversely, when the centre of the semicircle lies below the real axis, it signifies a diverse distribution of relaxation times[155].

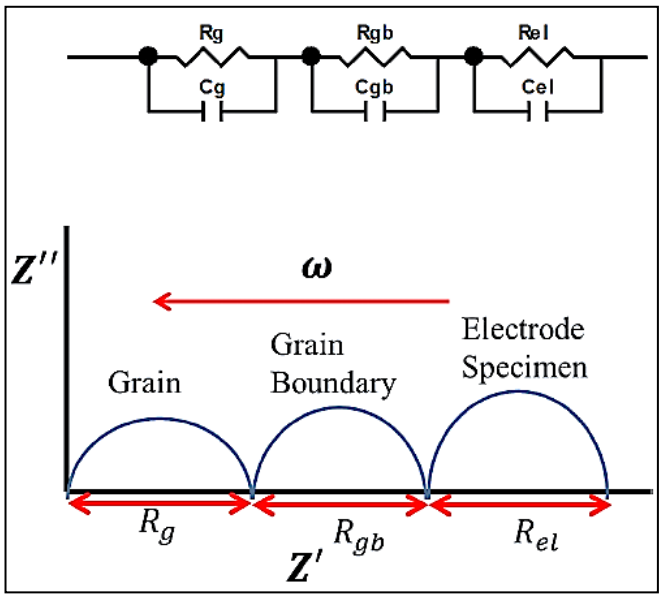


**Figure 2.14** The equivalent circuit corresponds to the polycrystalline sample and their frequency response in the complex impedance plot.

Sometimes, the impedance arc is depressed which leads to the necessity of a constant phase element (CPE)[156]. CPE is introduced to evaluate the deviation from the ideal impedance data. The CPE is expressed by the relation

$$Q_{CPE} = Q_o(j\omega)^{1/n} \tag{2.19}$$

where, n is frequency-independent and values lies in between 0 and 1. For the pure capacitive behavior value of '$n$' is unity and zero for the pure resistive behavior. This values of '$n$' can

be calculated from the slope of log-log plot of $|Z|$ and $\nu$ in the high-frequency regime[157]. In general, the '$n$' value determines the microstructure of the sample. In the present work, '$n$' value changes with the temperature, which can be attributed to the formation of ionic charge carriers.

## 2.5 Electrochemical Techniques

### 2.5.1 Electrode preparation

All the electrochemical studies were performed using a three-electrode setup available in the lab. The working electrode is the sample with ohmic contact. It is the electrode where the main electrochemical reaction takes place and placed at the center of other two electrode. A platinum (Pt) wire is used as the counter electrode for all the electrochemical measurements involving oxidation or reduction reactions. Its surface area needs to be greater than that of the working electrode to observe better kinetic reactions. An Ag/AgCl (3M KCl) electrode was used as the reference electrode in this three-electrode setup, acting as the fixed voltage source. It must be non-polarizable and capable of maintaining a consistent potential throughout the experiment, thereby allowing comparison of the working electrode's potential compared to it as a reference. The choice of electrode totally depends upon the type of solvent, the supporting electrolyte, and the sample used in the experiment.

Here, all the electrochemical measurements for the studies of OER, ORR and HER were performed on Metrohm Multichannel-autolab and Keithley 2450 source meter, using three-electrode setups as shown in Fig 2.15.

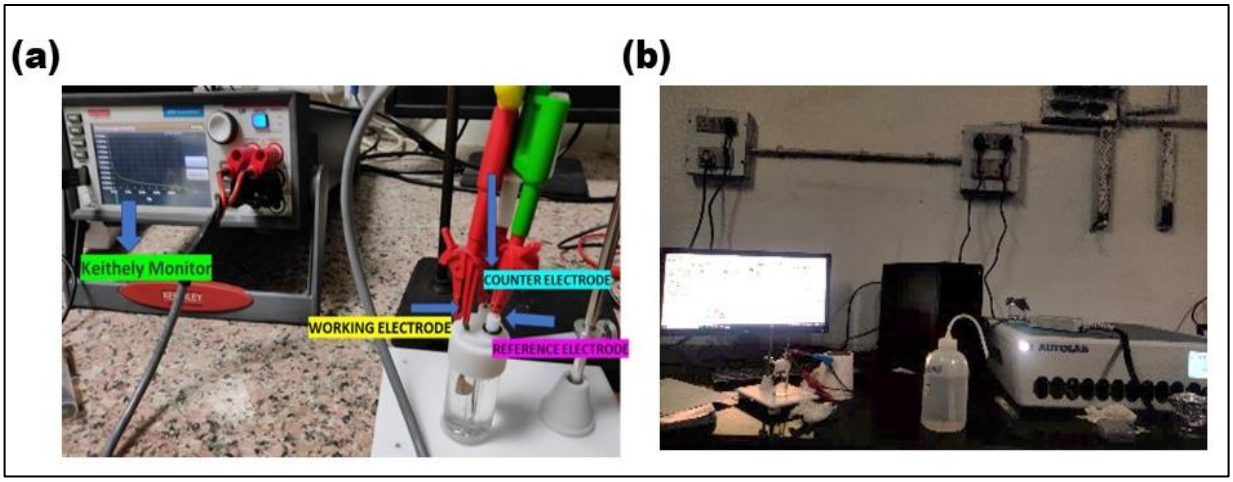


**Figure 2.15** Experimental set-up used for the electrochemical measurements **(a)** Keithley 2450 source meter **(b)** Multichannel Autolab PGSTAT – Metrohm with three electrode set-up.

### 2.5.2 Cyclic Voltammetry (CV)

CV is the most frequently used electrochemical technique for measuring the current response of a redox-active solution. It uses a three-electrode setup consisting of a working electrode, reference electrode, and counter electrode (refer to Fig 2.15). All three electrodes were immersed in a desired electrolyte solution. Here, the electrode is scanned in a cyclic potential range (in this work -1.5V to -1.5V), can be used for the qualitative and quantitative information of the electrochemical reactions[158]. Fig 2.16 shows the current -potential curve of CV, which can be measured at various scan rates. It is used for the study of oxidation and reduction processes involved in the sample and is essential for studying chemical reactions initiated by electron transfer, such as catalysis processes. CV studies were performed to examine the electrochemically active surface area of the working electrode, revealing the intrinsic surface area of the catalyst[158]. For a reversible electrochemical reaction, these curves have specific characteristics.

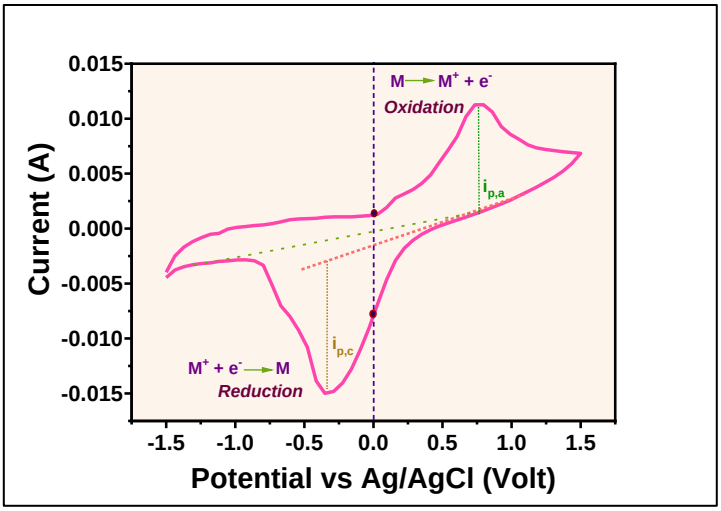


**Figure 2.16** Current-potential curve of a CV measurement

In the present thesis, the CV has been used to evaluate OER, ORR and HER mechanism process.

### 2.5.3 Linear Sweep Voltammetry (LSV)

Similar to CV, it also employs the three-electrode configuration. The only difference from the CV is the potential between the working electrode and a reference electrode is swept linearly in time and the current at the working electrode is measured (refer Fig 2.17). It can also be measured at different scan rate during the experiment. The characteristics of LSV curve depend on the rate of electron transfer reaction and on the chemical reactivity of the electroactive species.

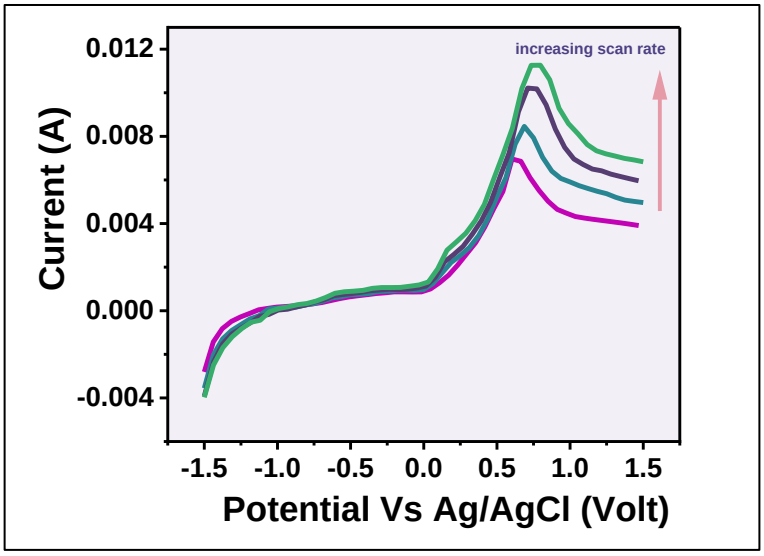


**Figure 2.17** Current-potential curve of a LSV measurement.

### 2.5.4 Tafel Plot

Tafel plot is the log-log plot of the current density and potential. It can be utilized to obtain the tafel slope and the charge transfer coefficient ($\alpha$), derived from the Butler-Volmer equation and expressed as:

$$\alpha = \beta \frac{RT}{nF} \tag{2.20}$$

where $\alpha$ is charge transfer coefficient, $R$ is the gas constant, $T$ is the value of room temperature, $n$ is number of electron transfer and $F$ is the faraday's constant, $\beta$ is the Tafel slope and values lie in between 0 to 1[159], [160].

It can be used to evaluate the reaction kinetics and $O_2$ adsorption mechanism on the catalyst's surface. This can also be used to compare the activity of various catalysts in both OER and ORR. Its value depends on the measurement conditions, including the applied scan rate and the scan direction of the curve. It can also be used to measure the corrosion rates of electrocatalyst materials[161].

### 2.5.5 Stability Test

The stability test was carried out through chrono-potentiometry measurements at a fixed current. chronopotentiometry involves potential variation over time at a fixed input current. This constant current is applied to the working electrode with respect to the counter electrode, and the corresponding potential is measured between the reference and working electrodes. The ideal catalysis for the ORR and OER or HER demands high stability for any practical application[162]. These experimental procedures revealed the long-term performance of the catalyst.

The chrono-amperometry test were also conducted at a fixed potential (in this work, taken as 2V) to obtain the current response as a function of time. Faradic reactions occur at the surface of working electrode and allows the current to flow. It is used to study the electroctalytic activity and stability at a specific potential. Efficient catalysts are characterized by their ability to sustain higher current values over an extended testing period, indicating better current retention. Diffusion coefficient of electroactive species of the catalyst or the surface area using the Shoup -Szabo realtion, given as follows-

$$I = \pi \mathrm{F} a n_c CD \left[1 + \left(\frac{P}{\pi}\right)^{\frac{1}{2}} + 0.2732\, exp\left(-0.391(P)^{\frac{1}{2}}\right)\right] \quad (2.21)$$

with $P \equiv \frac{a^2}{Dt}$

where $I$ is the diffusion current, $F$ is the Faraday constant, $a$ is the radius of the disk electrode, $n_c$ represents the charge number of the electrode reaction, $C$ is the concentration of the electroactive species, $D$ represents diffusion coefficient, and $t$ is the electrolysis time[163].

## 2.6 Analysis Techniques

### 2.6.1 Rietveld Refinement Technique

The Rietveld refinement was conducted to precisely determine the structural information and the crystallographic parameters. This technique is extensively used for microstructural and quantitative phase information of any material[164]. Rietveld's refinement method employed to simulate theoretically XRD data with the available crystal structure file named Crystallographic Information File (CIF). Refining structural and microstructural parameters involves maintaining fixed instrumental correction parameters. This refinement process occurs iteratively to match the experimental XRD pattern until all parameters converge. Successive refinements of the XRD patterns provide the best fit value between calculated (simulated) and experimental (observed) intensities.

A representative of the Rietveld refinement for the X-ray data is shown in Fig 2.18.

There are a number of software otions available for the studying the correlation between experimental and calculated patterns. In this work, the FullProf Suite has been employed for the refinement of the XRD patterns of the sample.

There are some important feature and advantage of this software listed below:

1. Quantitative phase analysis and crystalline structure.
2. Percentage of crystallinity for partially crystalline materials.
3. Unit cell size determination of material
4. FWHM parameters and crystallite size analysis
5. Chemical composition information

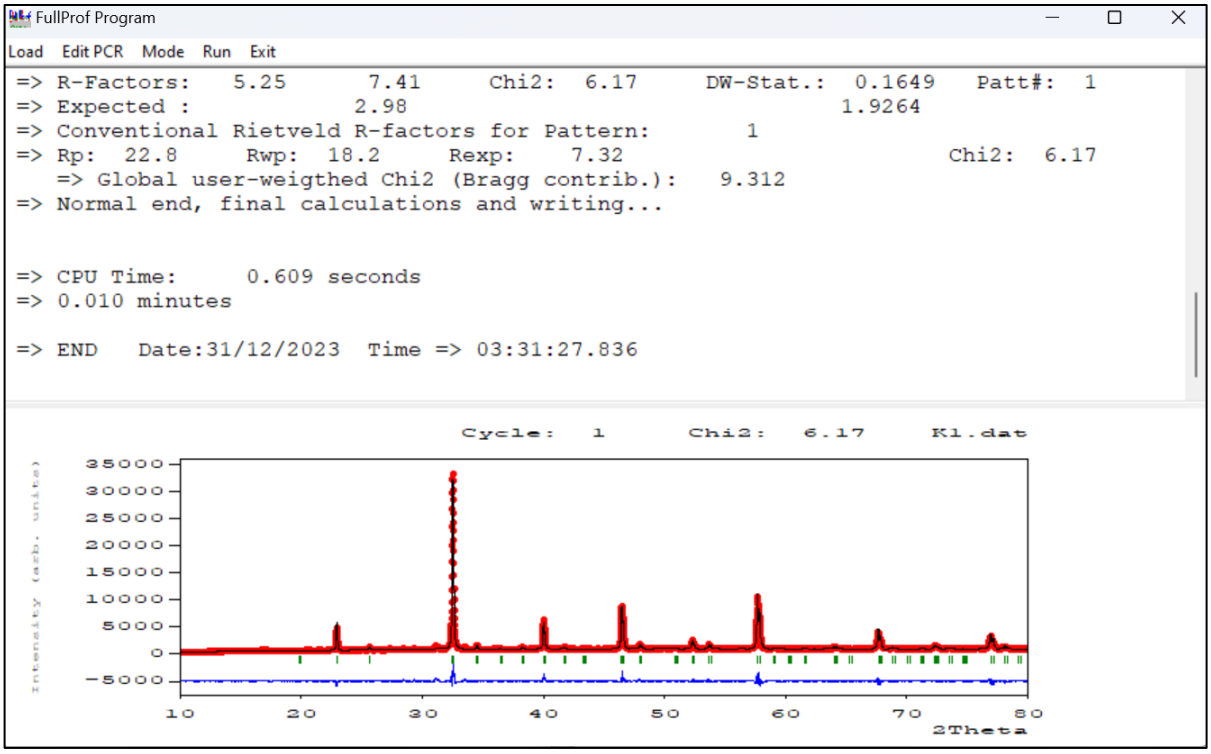


**Figure 2.18** Representative image of structural refinement fit of XRD data using FullProf Suite of the $LaFeO_3$.

## 2.6.2 Process of Analyzing the Obtained Data

Origin Pro 8.5 program, Image-J software, XPS41, and ZsimpWin were used to examine the structural, optical, and electrical aspects of the tested samples.